Pseudomonas aeruginosa contracts mucus to rapidly form biofilms in tissue-engineered human airways

Authors:

Tamara Rossy[1,2], Tania Distler[1,2], Joern Pezoldt[2], Jaemin Kim[3], Lorenzo Talà[1,2], Nikolaos Bouklas[3], Bart Deplancke[2], Alexandre Persat[1,2]

Affiliations:

[1] Global Health Institute, School of Life Sciences, École Polytechnique Fédérale de Lausanne (EPFL), Lausanne, Switzerland

[2] Institute of Bioengineering, School of Life Sciences, École Polytechnique Fédérale de Lausanne (EPFL), Lausanne, Switzerland

[3] Sibley School of Mechanical and Aerospace Engineering, Cornell University, Ithaca, NY, USA

Correspondence: alexandre.persat@epfl.ch

Abstract

Bacteria commonly protect themselves by forming multicellular structures called biofilms. The opportunistic pathogen *Pseudomonas aeruginosa* causes antibiotic-recalcitrant pneumonia by forming biofilms in the respiratory tract. Despite extensive *in vitro* experimentation, how *P. aeruginosa* forms biofilms at the airway mucosal surface is unresolved. We investigated *P. aeruginosa* biofilm biogenesis in optically-accessible tissue-engineered human lung models that emulate the airway mucosal environment. We found that *P. aeruginosa* forms mucus-associated biofilms within hours, much faster than previously observed in *in vitro* experiments. Early during colonization, *P. aeruginosa* induces contractions of luminal mucus which accelerates bacterial aggregation. We show that *P. aeruginosa* uses retractile type IV pili to actively compress mucus. Our results suggest that, while protecting epithelia, mucus constitutes a breeding ground for biofilms.

Main text

Bacteria predominantly colonize their environments in the form of biofilms, dense communities of contiguous cells embedded in a self-secreted polymeric matrix[1]. The mechanisms of biofilm formation have been extensively studied on abiotic surfaces and in laboratory conditions[2,3]. In contrast, our understanding of biofilm formation and physiology in a realistic context of human infections is limited[4,5]. Biofilms from the pathogen *P. aeruginosa* epitomize this disparity. *P. aeruginosa* causes acute and chronic pneumoniae in immunocompromised individuals by forming airway-associated biofilms[6]. The architecture of *P. aeruginosa* biofilms sampled from patient sputum and lung explants is quite different from *in vitro* ones[5]. This divergence indicates that airway mucosal factors that contribute to *P. aeruginosa* biofilm formation *in vivo* are omitted from laboratory investigations.

Epithelial tissues secrete a hydrogel substance called mucus, the first line of defense of the airway against all respiratory pathogens. Mucus is composed of gel-forming mucin glycoproteins, which cross-link into a viscoelastic substance upon exocytosis. It is commonly assumed that mucus is a passive physical barrier. However, bacterial pathogens and commensals physiologically adapt to mucins, suggesting mucus plays a regulatory role in host-microbe interactions. For example, glycans that decorate mucins regulate *P. aeruginosa* physiology, including virulence and adhesion[7]. Less is known about the regulatory role of mucus in its hydrogel form[8]. Individuals with underlying respiratory conditions such as chronic obstructive pulmonary disease (COPD) and cystic fibrosis (CF) have aberrant mucus. At the same time, they are at risk of specifically developing chronic *P. aeruginosa* pneumonia[9]. Despite this common association, how mucus mechanics contribute to the onset and persistence of *P. aeruginosa* infection remains unresolved. Mucus in its hydrogel form is fragile as it loses integrity upon mechanical and chemical perturbations[10,11]. As a result, mucus is largely omitted from investigations of *P. aeruginosa* biofilm formation. Consequently, we still ignore how *P. aeruginosa* interacts with native mucus to form biofilms during infection.

To bridge the gap between *in vitro* biofilm studies and clinical observations, we emulated the mucosal environment of the airway in the lab. We used a tissue-engineering approach to develop AirGels (airway in gels): human lung epithelial tissue in a molded collagen/Matrigel extracellular matrix (ECM) scaffold[12,13]. AirGels grow from primary human bronchial epithelial (HBE) cells of healthy and CF donors, which expand to confluence on the cylindrical cavity of the ECM scaffold (Figure 1A). An elastomeric microfluidic chip maintains AirGels and allows for luminal access while preserving epithelial integrity. The ECM geometry guides epithelial architecture, enabling morphological customization of AirGels. Here, we designed and optimized AirGels to enable high resolution fluorescence microcopy to monitor infection

dynamics at the single bacterium level in live tissue. Maintaining an air-liquid interface in the lumen promotes epithelial cell differentiation and reproduces the physiological conditions encountered in the airway. We therefore optimized the matrix formulation so that AirGels remain stable at the air-liquid interface, thereby biologically and physically replicating the airway environment (Figure 1B).

Single-plane illumination microscopy images show that mature AirGels form tubular epithelial tissue, recapitulating the architecture and dimensions of a human small bronchus (Figure 1C)[14,15]. AirGel epithelia are tight and impermeable (Supplementary Figure 1). We characterized HBE cell differentiation in 34-day-old AirGels. Immunofluorescence highlighted an abundant population of mucus-producing goblet cells and ciliated cells (Figure 1C). To quantify the abundance of each cell type, we performed single-cell RNA sequencing (scRNA-seq) of mature AirGels. We identified five main clusters (Figure 1D and Supplementary Figure 2): basal cells (8%), ciliated cells (41%), secretory cells (34%), as well as immature ciliated (7%) and immature secretory cells (10%). AirGels therefore reproduce the cellular composition and histological signature of human airway epithelia[16–19].

Given its prominent function in host-microbe interactions, we carefully characterized the architecture of mucus in AirGels. Immunofluorescence against the airway gel-forming mucins MUC5AC and MUC5B showed the presence of extracellular mucus in the form of thick luminal filaments (Figure 1E). We also observed similar fiber-like mucus architecture in live AirGels by staining with the fluorescently-labeled lectin jacalin[20]. These fibers recapitulate the mucus architecture observed in porcine and murine tracheal explants[20–22]. We then characterized AirGel mucociliary clearance functions. Measurements of cilia beating frequency in AirGels were indistinguishable from previous *ex vivo* measurements (Supplementary Figure 3 & Supplementary Video 1)[23–26]. In addition, AirGel cilia generated a directional flow whose clearance velocity matched the physiological range (Figure 1F)[22,24,27]. Overall, AirGels reproduce biological, physical and dynamic parameters of the human airway including its tube-shape, all in a system allowing for live imaging of host-pathogen interactions at high resolution.

To visualize biofilm formation in a realistic airway mucosal context, we inoculated *P. aeruginosa* constitutively expressing the fluorescent protein mScarlet in the lumen of AirGels maintained at the air-liquid interface. After 13h of incubation, we observed that bacteria had extensively colonized the mucosal surface. *P. aeruginosa* formed interconnected bacterial clusters colocalized with mucus within the airway surface liquid (ASL) between epithelial cells and the air-liquid interface (Figure 1G). In dynamic visualizations, bacteria remained attached to mucus despite mucus movements induced by beating cilia (Supplementary Video 2). Since *P. aeruginosa* takes days to form biofilms *in vitro*, we were surprised to see these communities

form only within a few hours in AirGels[28]. We therefore went on to investigate the mechanisms of rapid biofilm formation on mucus.

We imaged biofilm biogenesis in AirGels at the single cell level using confocal spinning disk microscopy. *P. aeruginosa* already formed aggregates a few hours after inoculation (Figure 2A). While the mucus surface was initially largely devoid of bacteria, half of it was covered by *P. aeruginosa* multicellular structures after 5.5h of infection (Figure 2B). Bacterial clusters with the same architecture also formed in the absence of jacalin staining, confirming these biofilms do not form through labeling artefacts (Supplementary Figure 4B). Moreover, *P. aeruginosa* rapidly formed biofilms on mucus of diseased AirGels engineered from primary cells of CF donors (Supplementary Figure 5). To confirm the pivotal role of mucus in rapid biofilm formation, we infected a non-differentiated AirGel which does not produce mucus. In the absence of a protective mucus layer, epithelial cells were more vulnerable to *P. aeruginosa* infection (Supplementary Figure 6). Bacteria breached through the epithelial barrier and invaded the underlying ECM. *P. aeruginosa* did not form three-dimensional multicellular structures in the ASL. This further demonstrates the role of mucus hydrogel as a substrate for biofilm formation in differentiated AirGels, and at the same time highlights its protective function.

Our data suggests that *P. aeruginosa* forms biofilms in the airway by attaching to mucus at early stages of infection. To further explore the biophysical mechanisms of biofilm formation, we harvested mucus to perform *ex situ* visualizations. However, we could not observe the formation of *P. aeruginosa* biofilms on mucus extracted from AirGels (Supplementary Figure 7 & Supplementary Video 3). We attribute this discrepancy to perturbations in mucus mechanical integrity when extracted from the epithelium. This difference highlights the importance of investigating microbe-mucus interactions in a native mucosal context such as the one established in AirGels.

To understand how biofilms rapidly form on native mucus, we therefore inspected the different steps of their formation in AirGels. To nucleate *in vitro* biofilms, *P. aeruginosa* cells navigate the surface of abiotic materials using twitching motility, which promotes the formation of aggregates[29]. Fast imaging of single cells shows that *P. aeruginosa* moves with twitching-like trajectories at the surface of mucus fibers (Supplementary Video 4). As expected from axenic experiments, these single cells aggregate into small clusters within 2h of colonization (Figure 2A). In contrast with axenic conditions, these small multicellular clusters subsequently moved along mucus fibers to eventually fuse (Figure 2C). This caused a cascade of cluster fusion events that sped up biofilm formation (Figure 2C & Supplementary Video 5). We tracked aggregate fusion in kymographs highlighting the correlation between mucus and bacterial

displacements (Figure 2D). The size of individual clusters remains approximately constant during motion and fusion, showing aggregate fusion predominates over bacterial growth. After only 6h of aggregation and fusion, dense biofilms are formed.

We found that during biofilm formation, the mucus surface area tends to decrease compared to an uninfected control (Figure 3A & Supplementary Figure 8). We therefore hypothesized that mucus gel remodeling could drive *P. aeruginosa* aggregation and aggregate fusion, thereby speeding up biofilm formation. We envisioned two mechanisms for bacteria-induced mucus deformations: degradation or direct mechanical contraction. *P. aeruginosa* secretes mucinases capable of degrading gel-forming mucins[30]. Enzymatic mucus degradation could release polymers that generate entropic depletion forces promoting bacterial aggregation or that generate osmotic forces compressing mucus[31,32]. To test whether mucus degradation could drive contraction, we colonized AirGels with a mutant in the type II secretion system locus *xcp* that is necessary for mucin utilization[30,33]. The *Δxcp* mutant however formed biofilms similar to WT, ruling out the hypothesis of polymer-induced forces driving the formation of multicellular structures (Figure 3B).

Could *P. aeruginosa* remodel mucus by directly and actively applying force on the surface? *P. aeruginosa* can generate extracellular forces using flagella and type IV pili (T4P), motorized filaments that also play a role during *in vitro* biofilm biogenesis. In addition, T4P and flagella mediate single cell interactions with mucins[34–38]. To investigate their functions in the context of rapid biofilm formation on mucus, we infected AirGels with *P. aeruginosa* mutants lacking flagella (*ΔfliC*) and T4P (*ΔpilA*). The *ΔfliC* mutant formed biofilms that were indistinguishable from wild type (WT) (Figure 3B). By contrast, *ΔpilA* cells did not form multicellular structures, indicating T4P play a role in rapid biofilm formation. Since T4P may bind to glycans present on mucins[37,38], weaker cell attachment to mucus could cause a decrease in aggregation of *ΔpilA*. Yet, colocalization analysis shows that the *ΔpilA* mutant is still able to attach efficiently to mucus (Supplementary Figure 9 & Supplementary Video 6). We therefore envisioned a mechanism where T4P generate retractile forces that contract mucus from the surface, ultimately speeding up *P. aeruginosa* aggregation and cluster fusion.

To physically explore this scenario, we ran non-linear finite element simulations wherein mucus is treated as a hyperelastic material[39]. The mechanical action of *P. aeruginosa* T4P at the mucus surface is considered through the introduction of an active surface stress. The simulations recapitulated the experimental observations of mucus hydrogel contraction during *P. aeruginosa* colonization (Figure 3C). Simulations also predict that the steady-state mucus area decreases with the magnitude of the surface contractile modulus. This suggests that the more T4P retract, the more *P. aeruginosa* compresses mucus. To experimentally validate this

model, we visualized AirGels colonization by a *ΔpilT* mutant which produces T4P that cannot retract, mimicking conditions of zero contractile modulus. *P. aeruginosa ΔpilT* could still associate with mucus and form a few small clusters, but clearly failed to form mucus-associated biofilms to the same extent as WT (Figures 3D & E), which was coherent with simulations. These results show that T4P retraction is necessary for rapid biofilm formation, and is consistent with a scenario where retraction compresses the mucus substrate.

To further support the surface contraction model, we tested the prediction that deformations increase further with surface contractility. We imaged AirGel colonization by the hyperpiliated *P. aeruginosa* mutant *ΔpilH,* whose T4P retraction frequency is approximately twice the one of WT (Supplementary Figure 10). *ΔpilH* formed biofilms more rapidly than WT: we observed dense aggregates as early as 2h, while we only did after 4h for WT (Figure 3F & G). In addition, *ΔpilH* induced more rapid mucus contraction than WT (Figure 3H & Supplementary Videos 7 & 8), consistent with simulations. After 5.5h, WT and *ΔpilH* biofilms had similar morphologies and size, suggesting biofilm fusion reaches a physical limit most likely due to packing at the mucus surface (Figure 3F and G). Overall, our results support a model where *P. aeruginosa* contracts the surface of mucus by active T4P retraction. Single cells initially twitch on mucus to form small aggregates. The static aggregate collective generate force from T4P that are sufficient to deform their substrate, driving large-scale mucus contraction. By contracting, mucus brings aggregates closer. They eventually fuse and form biofilms (Supplementary Figure 11).

Active mucus contraction by *P. aeruginosa* speeds up biofilm formation compared to axenic conditions. Although the classical view of airway infections associates biofilms with chronic infections and planktonic cells with acute infections, recent work has demonstrated the coexistence of these bacterial lifestyles in sputum samples from both acutely and chronically infected patients[40]. Our observations of rapid biofilm formation in both healthy and CF AirGels is consistent with these clinical observations.

Rapid biofilm formation may provide a fitness advantage in the non-hospitable airway environment. Forming biofilms rapidly could reduce *P. aeruginosa*'s susceptibility to neutrophils and macrophages, which are rapidly recruited to the mucosal surface during infection[41,42]. At the same time, forming biofilms increases *P. aeruginosa* tolerance to subsequent antibiotic treatment and promotes the emergence of resistant mutants[43]. There is however an upside: mucus adsorbs a large proportion of the planktonic *P. aeruginosa*, thereby shielding the epithelium from acute virulence. Our results therefore demonstrate the duality of mucus: protecting the airway epithelium from acute infections, while providing a fertile ground

for biofilm formation and chronic infections. Altogether, our study emphasizes the importance of investigating bacterial physiology in more realistic infection contexts.

Acknowledgements

We thank Zaïnebe Al-Mayyah, Jeremy Wong, the Bioimaging and Optics Core Facility (BIOP) and the Gene Expression Core Facility (GECF) at EPFL for technical assistance. Marco Kühn, Johannes Bues and Sophia Hsin-Jung Li for insightful discussions, Romé Voulhoux for strains and Formlabs forum user Telliria for suggestions on 3D-printing process. We acknowledge the Swiss National Science Foundation for funding this project through the Project grant number 310030_189084 and NCCR AntiResist.

References

1. Flemming, H.-C. *et al.* Biofilms: an emergent form of bacterial life. *Nature Reviews Microbiology* **14**, 563–575 (2016).
2. Teschler, J. K. *et al.* Living in the matrix: assembly and control of Vibrio cholerae biofilms. *Nat Rev Microbiol* **13**, 255–268 (2015).
3. Yan, J. & Bassler, B. L. Surviving as a Community: Antibiotic Tolerance and Persistence in Bacterial Biofilms. *Cell Host & Microbe* **26**, 15–21 (2019).
4. Costerton, J. W., Stewart, P. S. & Greenberg, E. P. Bacterial biofilms: a common cause of persistent infections. *Science* **284**, 1318–1322 (1999).
5. Bjarnsholt, T. *et al.* The in vivo biofilm. *Trends in Microbiology* **21**, 466–474 (2013).
6. Rossi, E. *et al.* Pseudomonas aeruginosa adaptation and evolution in patients with cystic fibrosis. *Nat Rev Microbiol* **19**, 331–342 (2021).
7. Wheeler, K. M. *et al.* Mucin glycans attenuate the virulence of Pseudomonas aeruginosa in infection. *Nature Microbiology* **4**, 2146–2154 (2019).
8. Matsui, H. *et al.* A physical linkage between cystic fibrosis airway surface dehydration and Pseudomonas aeruginosa biofilms. *Proceedings of the National Academy of Sciences* **103**, 18131–18136 (2006).
9. Folkesson, A. *et al.* Adaptation of Pseudomonas aeruginosa to the cystic fibrosis airway: an evolutionary perspective. *Nature Reviews Microbiology* **10**, 841–851 (2012).

10. Wagner, C. E., Wheeler, K. M. & Ribbeck, K. Mucins and Their Role in Shaping the Functions of Mucus Barriers. *Annual Review of Cell and Developmental Biology* **34**, 189–215 (2018).

11. Perez-Vilar, J. & Mabolo, R. Gel-forming mucins. Notions from in vitro studies. *Histol. Histopathol.* **22**, 455–464 (2007).

12. Jiménez-Torres, J. A., Peery, S. L., Sung, K. E. & Beebe, D. J. LumeNEXT: A Practical Method to Pattern Luminal Structures in ECM Gels. *Advanced Healthcare Materials* **5**, 198–204 (2016).

13. Barkal, L. J. *et al.* Microbial volatile communication in human organotypic lung models. *Nature Communications* **8**, 1770 (2017).

14. Chen, Y. *et al.* Validation of human small airway measurements using endobronchial optical coherence tomography. *Respiratory Medicine* **109**, 1446–1453 (2015).

15. Horsfield, K. & Cumming, G. Morphology of the bronchial tree in man. *Journal of Applied Physiology* **24**, 373–383 (1968).

16. Dvorak, A., Tilley, A. E., Shaykhiev, R., Wang, R. & Crystal, R. G. Do Airway Epithelium Air–Liquid Cultures Represent the In Vivo Airway Epithelium Transcriptome? *Am J Respir Cell Mol Biol* **44**, 465–473 (2011).

17. Montoro, D. T. *et al.* A revised airway epithelial hierarchy includes CFTR-expressing ionocytes. *Nature* **560**, 319–324 (2018).

18. Plasschaert, L. W. *et al.* A single-cell atlas of the airway epithelium reveals the CFTR-rich pulmonary ionocyte. *Nature* **560**, 377–381 (2018).

19. Travaglini, K. J. *et al.* A molecular cell atlas of the human lung from single-cell RNA sequencing. *Nature* **587**, 619–625 (2020).

20. Ostedgaard, L. S. *et al.* Gel-forming mucins form distinct morphologic structures in airways. *PNAS* **114**, 6842–6847 (2017).

21. Hoegger, M. J. *et al.* Impaired mucus detachment disrupts mucociliary transport in a piglet model of cystic fibrosis. *Science* **345**, 818–822 (2014).

22. Fakih, D. *et al.* Normal murine respiratory tract has its mucus concentrated in clouds based on the Muc5b mucin. *American Journal of Physiology-Lung Cellular and Molecular Physiology* **318**, L1270–L1279 (2020).

23. Hoegger, M. J. *et al.* Assessing mucociliary transport of single particles in vivo shows variable speed and preference for the ventral trachea in newborn pigs. *PNAS* **111**, 2355–2360 (2014).

24. Fahy, J. V. & Dickey, B. F. Airway mucus function and dysfunction. *New England Journal of Medicine* **363**, 2233–2247 (2010).

25. Bermbach, S. *et al.* Mechanisms of Cilia-Driven Transport in the Airways in the Absence of Mucus. *Am J Respir Cell Mol Biol* **51**, 56–67 (2014).

26. Rayner, R. E., Makena, P., Prasad, G. L. & Cormet-Boyaka, E. Optimization of Normal Human Bronchial Epithelial (NHBE) Cell 3D Cultures for in vitro Lung Model Studies. *Scientific Reports* **9**, 500 (2019).

27. Kudo, E. *et al.* Low ambient humidity impairs barrier function and innate resistance against influenza infection. *PNAS* **116**, 10905–10910 (2019).

28. Ma, L. *et al.* Assembly and Development of the Pseudomonas aeruginosa Biofilm Matrix. *PLOS Pathogens* **5**, e1000354 (2009).

29. Zhao, K. *et al.* Psl trails guide exploration and microcolony formation in Pseudomonas aeruginosa biofilms. *Nature* **497**, 388–391 (2013).

30. Alrahman, M. A. & Yoon, S. S. Identification of essential genes of Pseudomonas aeruginosa for its growth in airway mucus. *J Microbiol.* **55**, 68–74 (2017).

31. Datta, S. S., Preska Steinberg, A. & Ismagilov, R. F. Polymers in the gut compress the colonic mucus hydrogel. *Proceedings of the National Academy of Sciences* **113**, 7041–7046 (2016).

32. Secor, P. R., Michaels, L. A., Ratjen, A., Jennings, L. K. & Singh, P. K. Entropically driven aggregation of bacteria by host polymers promotes antibiotic tolerance in Pseudomonas aeruginosa. *Proceedings of the National Academy of Sciences* **115**, 10780–10785 (2018).

284 33. Chapon-Hervé, V. *et al.* Regulation of the *xcp* secretion pathway by multiple quorum-
285 sensing modulons in *Pseudomonas aeruginosa*. *Molecular Microbiology* **24**, 1169–1178
286 (1997).
287 34. Co, J. Y. *et al.* Mucins trigger dispersal of Pseudomonas aeruginosa biofilms. *NPJ*
288 *Biofilms Microbiomes* **4**, (2018).
289 35. Arora, S. K., Ritchings, B. W., Almira, E. C., Lory, S. & Ramphal, R. The Pseudomonas
290 aeruginosa Flagellar Cap Protein, FliD, Is Responsible for Mucin Adhesion. *Infect Immun*
291 **66**, 1000–1007 (1998).
292 36. Landry, R. M., An, D., Hupp, J. T., Singh, P. K. & Parsek, M. R. Mucin–Pseudomonas
293 aeruginosa interactions promote biofilm formation and antibiotic resistance. *Molecular*
294 *Microbiology* **59**, 142–151 (2006).
295 37. Comolli, J. C., Waite, L. L., Mostov, K. E. & Engel, J. N. Pili Binding to Asialo-GM1 on
296 Epithelial Cells Can Mediate Cytotoxicity or Bacterial Internalization by Pseudomonas
297 aeruginosa. *Infect Immun* **67**, 3207–3214 (1999).
298 38. Bucior, I., Pielage, J. F. & Engel, J. N. Pseudomonas aeruginosa Pili and Flagella
299 Mediate Distinct Binding and Signaling Events at the Apical and Basolateral Surface of
300 Airway Epithelium. *PLOS Pathogens* **8**, e1002616 (2012).
301 39. Kim, J., Mailand, E., Ang, I., Sakar, M. S. & Bouklas, N. A model for 3D deformation
302 and reconstruction of contractile microtissues. *Soft Matter* **17**, 10198–10209 (2021).
303 40. Kolpen, M. *et al.* Bacterial biofilms predominate in both acute and chronic human lung
304 infections. *Thorax* (2022) doi:10.1136/thoraxjnl-2021-217576.
305 41. Montefusco-Pereira, C. V. *et al.* P. aeruginosa Infected 3D Co-Culture of Bronchial
306 Epithelial Cells and Macrophages at Air-Liquid Interface for Preclinical Evaluation of Anti-
307 Infectives. *JoVE (Journal of Visualized Experiments)* e61069 (2020) doi:10.3791/61069.
308 42. Yonker, L. M. *et al.* Development of a Primary Human Co-Culture Model of Inflamed
309 Airway Mucosa. *Sci Rep* **7**, 8182 (2017).
310 43. Ciofu, O., Moser, C., Jensen, P. Ø. & Høiby, N. Tolerance and resistance of microbial
311 biofilms. *Nat Rev Microbiol* 1–15 (2022) doi:10.1038/s41579-022-00682-4.

Figures

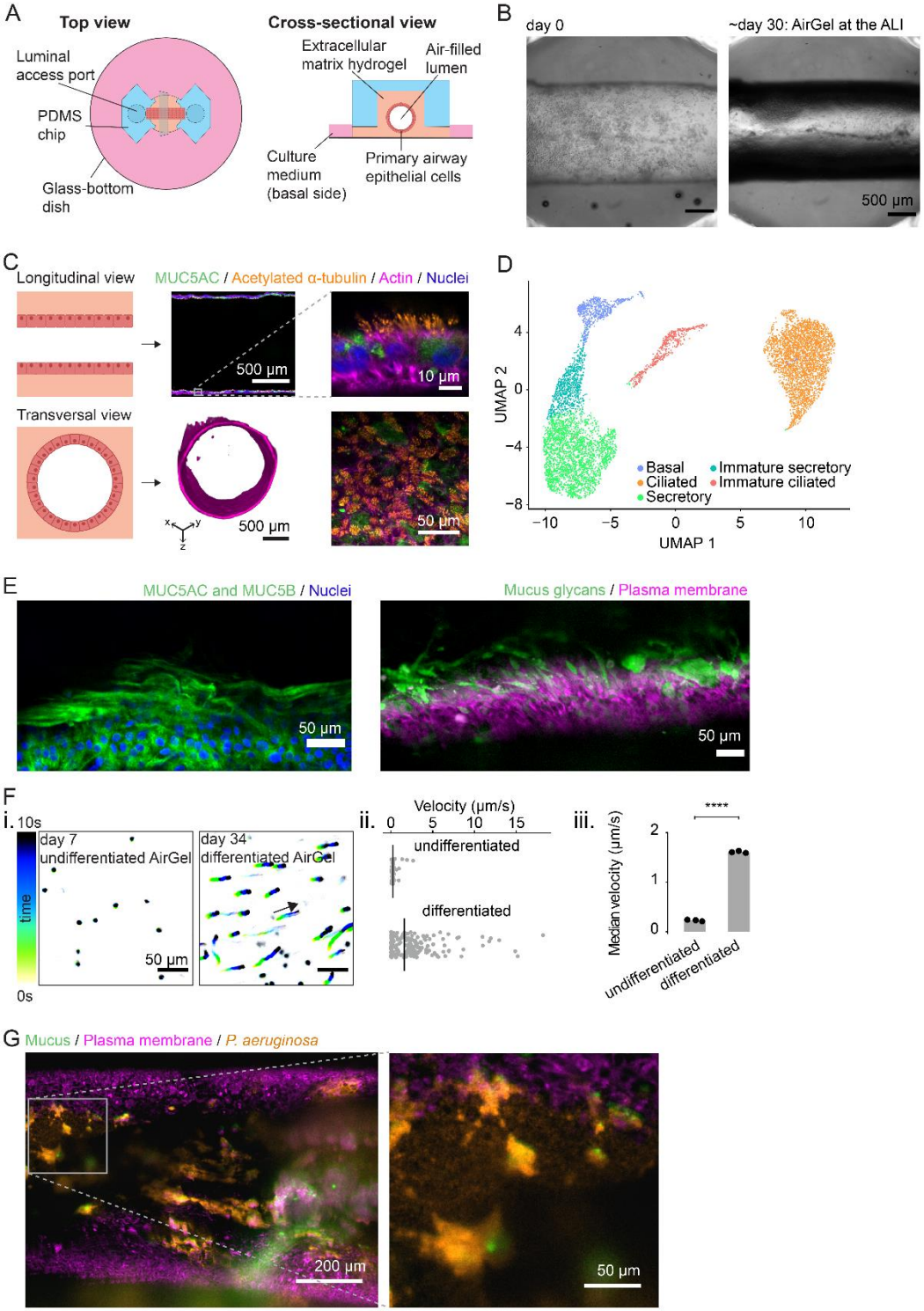

Figure 1: A tissue-engineered airway as a novel infection model. A. Schematic of an AirGel chip. **B.** Brightfield image of an AirGel on the day of HBE cell were seeding (left) and at the air-liquid interface after 30 days in culture (right). **C.** Longitudinal cross-sectional images of immunostained differentiated AirGel chips. Confocal images show the gel-forming mucin MUC5AC (green) and acetylated α-tubulin labeling cilia (orange) along with the actin dye

phalloidin (pink) and nuclear dye DAPI (blue). The transverse cross section 3D image was reconstituted from SPIM data for actin fluorescence. The bottom right panel is a maximal intensity projection of a z-stack acquired in the curved lumen. **D.** scRNA-seq identifies cell type diversity of AirGels. Uniform Manifold Approximation and Projection (UMAP) embedding of cells pooled from three differentiated AirGels (35-days old), subjected to scRNA-seq profiling. **E.** Extracellular luminal mucus in AirGels. Immunofluorescence of methacarn-fixed AirGels shows the presence of extracellular MUC5AC and MUC5B gel-forming mucins (left). The fluorescent lectin jacalin, which targets glycans, labels extracellular mucus in AirGels (right). **F.** Mucociliary clearance in AirGels. i. trajectories of fluorescent microparticles in the lumen of 7-day-old and 34-day-old AirGels. ii. corresponding velocity distributions. Black lines indicate the median velocity. iii. median particle velocities for three differentiated and undifferentiated AirGels show the contribution of cilia beating in clearance. Each data point corresponds to the median in each experiment; the gray bar shows the median of triplicates. Statistics: independent samples Student t-test with Bonferroni correction ($p < 10^{-7}$). **G.** *P. aeruginosa* infection of a 62-day-old cystic fibrosis AirGel. Confocal images were acquired 13h after inoculation. *P. aeruginosa* constitutively expresses the fluorescent protein mScarlet. The plasma membrane of epithelial cells was stained with CellMask Deep Red (pink). Mucus was stained with jacalin (green) shortly before infection.

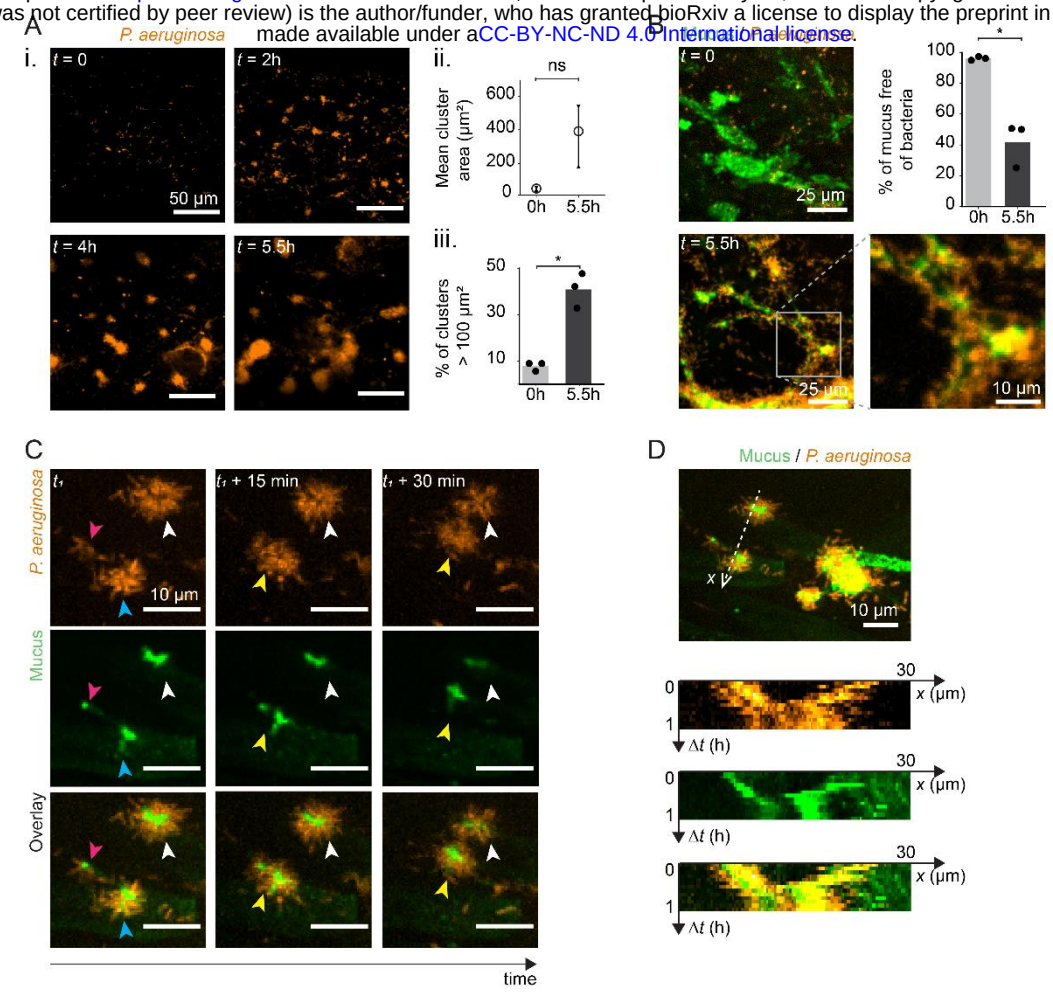

Figure 2: *P. aeruginosa* rapidly forms mucus-associated biofilms. A. i. maximal intensity projection images of *P. aeruginosa* in a 35-day-old AirGel (healthy donor) shows biofilm formation within hours. ii. mean biofilms cluster area for 3 AirGels. The bar indicates the range between the maximum and minimum of the three means. The circle represents the mean of the means. iii. percentage of clusters that were larger than 100 µm^2 in each replicate (black dots). The bars represent the mean across replicates. Statistics: paired samples Student t-test with Bonferroni correction ($p = 0.051$ and $p = 0.01$). **B.** *P. aeruginosa* rapidly colonizes mucus surfaces. Images show maximal intensity projection of confocal stacks of a 33-day-old infected AirGel at $t = 0$ and $t = 5.5$h post-inoculation. The graph quantifies the proportion of mucus not occupied by bacteria. Gray bars show the mean of triplicates. Statistics: paired samples Student t-test with Bonferroni correction ($p = 0.02$). **C.** Dynamic visualization of *P. aeruginosa* cluster fusion on mucus in a 33-day-old AirGel ($t_1 = 6.2$h). The blue and pink arrowheads show two aggregates that fuse within the first 15 min. The resulting cluster is indicated by a yellow arrowhead. This new cluster then moves closer to the one indicated by the white arrowhead. All images are maximal intensity projections from z-stacks. **D.** Kymographs showing the displacement of two clusters along their axis of motion. The bacterial aggregate and underlying mucus traveled together at an approximate speed of 0.5 µm/min.

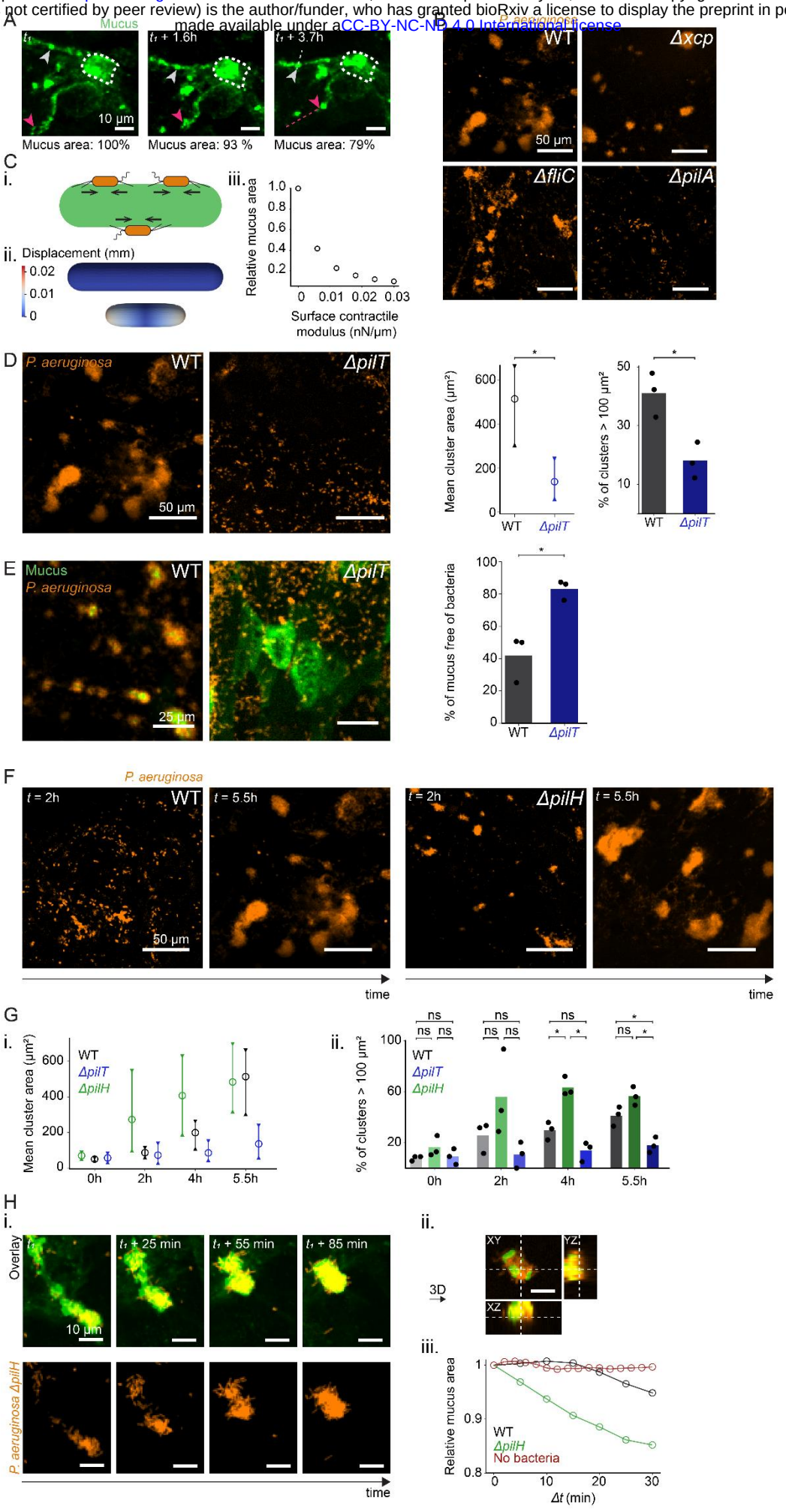

353 **Figure 3: Mucus contraction drives rapid biofilm formation. A.** Time course visualization

of a mucus patch in a 35-day-old AirGel infected with WT *P. aeruginosa* (t_1 = 1.2h). Reference features are indicated by colored arrowheads. Dashed lines show their trajectories. **B.** Biofilm formation of PAO1 mutants unable to degrade mucus or to generate force (t = 5.5h). The *Δxcp* mutant that lacks type II secretion system necessary for secretion of mucinases forms biofilms similar to WT. The *ΔfliC* mutant lacking flagella also formed WT-like biofilms. In contrast, the *ΔpilA* mutant lacking T4P was unable to form luminal biofilms in AirGels. **C.** Finite element simulations of mucus deformation during surface contraction. i. schematic representation of *P. aeruginosa* applying contractile force on mucus by retracting T4P. ii. finite element simulation of deformation of a mucus cylinder at rest (top) and under active surface stress (bottom). Colormap indicate displacement of surface elements. iii. relative mucus area as a function of surface contractile modulus. As the surface contractile modulus increases, the relative area of mucus decreases. **D.** T4P retraction is necessary for biofilm formation. Images compare biofilms from WT *P. aeruginosa* and from the *ΔpilT* mutant unable to retract T4P (t = 5.5h). *ΔpilT* cluster area and percentage of large clusters is much smaller than WT (N = 3). Statistics: independent samples Student t-test with Bonferroni correction (p = 0.035 and p = 0.015). **E.** Mucus does not rearrange during *ΔpilT* colonization (t = 5.5h). Most of the mucus surface remains free of bacteria during *ΔpilT* colonization (N = 3). Statistics: independent samples Student t-test with Bonferroni correction (p = 0.01). **F.** Increased T4P activity speeds up biofilm formation on mucus. Comparison of biofilm formation by the *ΔpilH* mutant with hyperactive T4P with WT, at t = 2h and t = 5.5h after inoculation. *ΔpilH* already forms small biofilms after 2h. **G.** i. kinetics of biofilm size for WT, *ΔpilT* and *ΔpilH*. For each strain, we infected three AirGels from a healthy donor. Bars represent the range between the maximum and minimum of the means from triplicates, circles represent the overall mean. ii. comparison of percentage of large clusters for WT, *ΔpilT* and *ΔpilH*, over time. Statistics: one-way ANOVA for each time point, followed by a post-hoc Tukey test if the null hypothesis was rejected. At t = 4h, the differences between WT and *ΔpilH* (p = 0.003) and between *ΔpilH* and *ΔpilT* (p = 0.001) were significant. At t = 5.5h, the differences between WT and *ΔpilT* (p = 0.02) and between *ΔpilH* and *ΔpilT* (p = 0.001) were significant. **H.** *ΔpilH* dramatically contracts mucus. i. timelapse confocal images showing a dynamic event of mucus contraction by *ΔpilH*. ii. orthogonal views of the bacteria-covered mucus cluster at t_1 + 85 min, showing that PAO1 *ΔpilH* cells surround mucus. iii. relative mucus area changes measured during a 30 min time interval for WT and *ΔpilH*; since *ΔpilH* starts aggregating and remodeling mucus earlier than WT, the starting points of the recording differed (*ΔpilH*: 2.5h, WT: 6.2h, negative control: 8.1h). Images are maximal intensity projections of z-stacks throughout the figure except for the orthogonal projection in H.